BioScatter: Low-Power Sweat Sensing with Backscatter

Wenli Jiao, Yanlin Li, Xiangdong Xi, Ju Wang*, Dingyi Fang, Xiaojiang Chen
Northwest University, China
Shaanxi International Joint Research Centre for the Battery-Free Internet of Things, China
{jiaowenli,yanlinli2579,way9890xxd}@stumail.nwu.edu.cn,{wangju,dyf,xjchen}@nwu.edu.cn

ABSTRACT

Sweat contains a wealth of physiologically relevant information and has been used to detect underlying diseases or the sub-health state. However, existing sweat sensors suffer from high energy consumption due to the need for energy-hungry components (i.e., ADC and DAC) and active radio front-ends, making them unable to support continuous and long-term monitoring.

This paper introduces BioScatter, a backscatter-based accurate and ultra-low-power sweat sensing wearable sensor that does not need any energy-hungry ADC, DAC, and active radios. The key to eliminating DAC is a novel low-power voltage sweeping circuit design that can perform as well as a 12-bit DAC. To eliminate the ADC, we borrow backscatter technology that can directly transmit the measured analog sensing values to the reader, thus avoiding digital sampling. Extensive results show that BioScatter has a low-power consumption of 313.5 μW and achieves more than 98.5% sensing accuracy for detecting five concentration levels of three types of important bio-fluid in sweat.

CCS CONCEPTS

• **Hardware → Wireless devices**; **Sensor devices and platforms**; • **Human-centered computing → Ubiquitous and mobile computing systems and tools**.

KEYWORDS

Wearable biosensors, Low-power, Sweat sensing, Backscatter, Internet of Things (IoT)

ACM Reference Format:
Wenli Jiao, Yanlin Li, Xiangdong Xi, Ju Wang*, Dingyi Fang, Xiaojiang Chen. 2023. BioScatter: Low-Power Sweat Sensing with Backscatter. In *ACM International Conference on Mobile Systems, Applications, and Services (MobiSys '23), June 18–22, 2023, Helsinki, Finland.* ACM, New York, NY, USA, 14 pages. https://doi.org/10.1145/3581791.3596834

1 INTRODUCTION

Sweat is an important bio-fluid since its composition can reveal changes in physiological indicators rapidly, and thus detect underlying diseases or the sub-health state [10, 19, 33, 50]. For example, uric acid (UA) concentration in sweat indicates a risk factor for cardiovascular disease [19, 20], type-2 diabetes [12, 33] and renal disease, and is widely used in clinical practice. For instance, ascorbic acid (AA) in sweat can help non-invasive assessment of health levels, because AA participates in many important physiological and biochemical functions, such as the synthesis of hormones and neurotransmitters, the metabolism of amino acids and vitamins, and the liver detoxification of toxins [30]. Moreover, excessive loss of sodium (Na^+) in sweat has been shown to be associated with an increased risk for hyponatremia [50]. Therefore, continuous and long-term monitoring can also allow us to detect the body's chronic diseases in time, such as high urea acid, cystic fibrosis, etc.

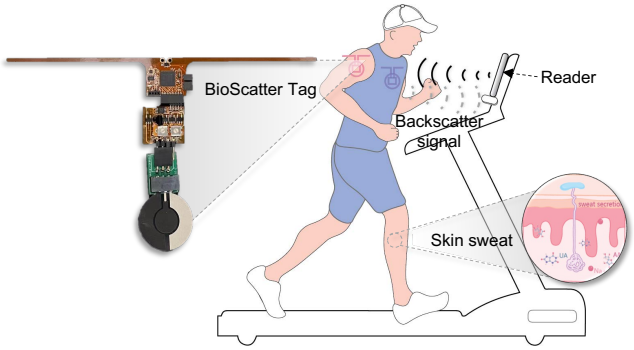

Figure 1: An example of BioScatter's application. The BioScatter tag is attached to the user's skin and a reader is equipped on the treadmill. The tag senses the skin's sweat and backscatters the signal to the reader.

To realize continuous and long-term sweat sensing, an ideal solution is to use wearable devices/sensors, due to the widely available smartphones and other mobile devices can easily and wirelessly collect sensing data from wearable devices, enabling personalized and long-term monitoring [10]. Although existing commercial smartwatch devices can monitor the physical signals (e.g., steps and heart rate) or blood oxygen concentration [6, 28], they cannot sense the fine-grained molecular level in sweat. Recently, several sweat sensors have been proposed [26, 56, 57]. However, they rely on high power consumption components (i.e., ADC and DAC) and active radio front-ends, making them unable to support continuous and long-term monitoring which is a fundamental requirement for wearable devices [1–3, 11].

In this paper, we propose BioScatter, a backscatter-based accurate and ultra-low-power sweat sensing wearable sensor that does not need any energy-hungry ADC, DAC, and active radios. Our BioScatter uses fully-analog components for sweat sensing, and battery-free, backscatter technology for sending data to remote devices. Fig. 1 shows an example application of BioScatter for monitoring the sweat when a person is exercising on a treadmill, where the sweat sensor (i.e., BioScatter tag) is attached to the human body

*Corresponding author.

MobiSys '23, June 18–22, 2023, Helsinki, Finland

ACM ISBN 979-8-4007-0110-8/23/06…$15.00
https://doi.org/10.1145/3581791.3596834

and a reader installed on the treadmill is used to activate the tag and acquire the sweat information.

The key challenge in BioScatter's design is how to eliminate the energy-hungry DAC and ADC components. Because traditional sweat sensors are not passive and require a sweeping voltage on the sensor's electrodes to catalyze the chemical reaction between the sweat and the electrodes. Then, the chemical reaction will produce different currents according to different sweat concentrations. Thus, one can detect sweat concentration by observing currents. Given this, fine-grained voltage sweeping is required for achieving accurate and high-resolution sweat sensing. Existing solutions use a digital-to-analog converter (DAC) for generating fine-grained voltage sweeping and an analog-to-digital (ADC) for sampling the sensing voltage. However, the DAC and ADC are energy-hungry [24], preventing continuous and long-term monitoring. For example, even for the state-of-the-art (SOTA) low-power micro-controller (e.g., MSP430), the power consumption will increase by 60% (i.e., 270 μW) when turning on its onboard DAC. Similarly, turning on ADC for sampling sensing data will increase power consumption by 73% (i.e., 370 μW) [52].

To eliminate the energy-hungry DAC, we design a novel analog low-power voltage sweeping circuit that can perform as well as a 12-bit DAC. Our basic idea is to exploit a pulse width-adjustable PWM signal (that is generated by a low-power MCU) and a second-order RC filter to emulate a sweeping voltage for the sweat sensor. However, the challenge is how to realize fine-grained voltage sweeping given the low-power constraint. Specifically, fine-grained voltage sweeping requires the voltage sweep step as small as possible, which however requires a high clock frequency and thus increases power consumption. To overcome this challenge, we take advantage of the long rising time between two voltage steps to emulate an approximate linear and fine-grained voltage sweeping, which differs from traditional PWM-based DAC circuits. To achieve this, we model the relationship between the design requirements and the circuit parameters as a group of inequalities. By solving inequalities and fine-tuning circuit parameters, we can obtain the optimal circuit parameters, and finally increase the resolution of our PWM-based voltage sweeping method by nearly 125×.

To eliminate the energy-hungry ADC component, we borrow the backscatter technology [42, 45, 49] that can directly transmit the measured analog sensing values to the reader, thus avoiding digital sampling. However, it is non-trivial to utilize backscatter in our system due to the well-known challenge: the supply voltage from backscatter energy harvesting is unstable [44, 59], resulting in significant sensing errors or even failure. To combat the supply voltage fluctuation, we design a fully passive supply voltage monitoring and calibration circuit, which can provide sweat sensors with a stable sweeping voltage that is close to the ideal one. Overall, we reduce the energy consumption in both the sensor (via eliminating DAC) and the communication (via bypassing ADC).

We built a prototype of BioScatter tag with a flexible PI substrate. The tag's overall power consumption is 313.5 μW. We have evaluated BioScatter on sensing three important substances in sweat, including urea acid (UA), ascorbic acid (AA), and Na^+. Extensive results show that BioScatter achieves more than 98.5% accuracy in detecting five concentration levels of UA or AA or Na^+, and achieves sensing resolutions of 8 $\mu mol/L$, 8 $\mu mol/L$, 20 $mmol/L$ for UA, AA, and Na^+. It is worth noting that our sensing resolution exceeds the requirement of medical needs since hospitals usually only need a three-level detection (i.e., normal level, below the normal level, and higher than normal level). The backscatter communication range of BioScatter can achieve up to 21 m.

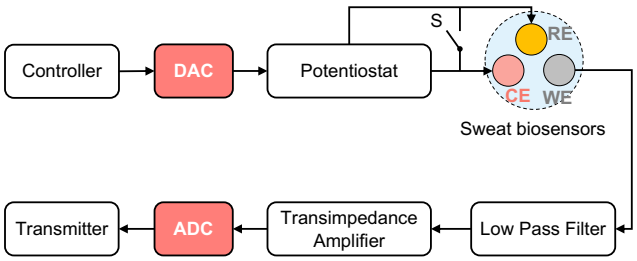

Figure 2: Traditional sweat sensing circuit.

Contributions. We propose a backscatter-based ultra-low-power sweat sensing wearable sensor that does not need the energy-hungry ADC, DAC, and active radios. We design a novel low-power voltage sweeping circuit that can perform as well as a 12-bit DAC. Other bio-sensors can use our circuit design to achieve low-power sensing without a DAC component. We design a fully passive supply voltage monitoring and calibration circuit to combat supply voltage fluctuation, which is a well-known challenge in backscatter-based battery-free systems.

2 BACKGROUND AND MOTIVATION

Background of the sweat sensing circuit. Fig. 2 shows a traditional sweat sensing system schematic [9]. To detect the urea acid (UA) and ascorbic acid (AA) molecule concentration in sweat, the controller outputs a digital signal to the digital-to-analog converter (DAC) to generate a sweeping voltage, which is applied to the potentiostat's counter electrode (CE), triggering a chemical reaction between the sweat biosensor's working electrode (WE) and the UA/AA molecules. The chemical reaction will induce a micro-current in the sweat and the circuit, whose magnitude is positively related to the UA/AA concentration. Then, the generated current is filtered by a lowpass filter, and amplified by a transimpedance amplifier. Next, the amplified voltage is sampled by an analog-to-digital converter (ADC). Finally, the transmitter sends the sampled digital signal to a remote reader via an active radio (Wi-Fi/Bluetooth).

Different from UA and AA detection, the standard method for Na^+ ions concentration detection is the open circuit potential method [9], which consists of two electrodes WE and RE. Specifically, the system closes the switch S to short the CE and RE and measures the voltage between WE and RE (as shown in Fig. 2), which is proportional to the Na^+ ions concentration. Thus, by measuring the open circuit voltage one can estimate Na^+ ions concentration. The sequential circuits are the same as the UA/AA detection.

As we can see, the traditional method for sensing sweat concentration requires the DAC, ADC, and active radios which are usually power-hungry. Table. 1 shows the power consumption of DAC, ADC, and active radios used in existing sweat sensing systems [21, 46, 56, 57]. We can see that the power consumption of these active components is sub-mW ~ tens of mW, which is higher

Table 1: Power consumption of DAC, ADC and active radios.

System	DAC	ADC	Active Radio	Voltage
NutriTrek [56]	1 mW	0.53 mW	39.6 mW	3.3 V
LEG-CS [57]	1 mW	0.53 mW	39.6 mW	3.3 V
Enactsense [46]	0.264 mW	1.04 mW	17.5 mW	3.3 V
FISA [21]	0.264 mW	0.313 mW	17.5 mW	5.0 V

than existing energy harvesting efficiency and thus not suitable for use in ultra-low-power applications that rely on energy harvesting.

Backscatter. Backscatter is a low-power communication method that passively reflects the incident carrier signal and modulates the tag's data on the reflection signal. By controlling the baseband signal's amplitude/phase/frequency/duty-cycle, one can modulate the carrier in different schemes such as OOK modulation [47], frequency modulation [54], and pulse interval modulation [49]. In this work, we select pulse interval modulation, which can combat mobile interference and achieve lower power consumption than frequency modulation.

Motivation. Hence, BioScatter aims to achieve ultra-low-power sweat sensing from two aspects: (i) eliminate the power-hungry DAC and ADC components, and (ii) leverage the passive backscatter communication. In the following sections, we will describe the system design to achieve the above goals, followed by detailed implementation and evaluation with extensive experiments.

3 BIOSCATTER DESIGN

In this section, we will first explain the sweat sensing principle. Next, we will detail how we eliminate the energy-hungry DAC and ADC to achieve low-power sensing. Finally, we will present the entire circuit diagram of BioScatter and explain the workflow for estimating sweat concentration.

3.1 Sweat Sensing Principle

In order to analyze the micro-level sweat concentration, the basic idea is to transduce the chemical energy into electric energy [7]. In this work, the target substances can be divided into two types, i.e., molecules (UA, AA) and ions (Na^+).

Sensing Principle of UA/AA Molecules. Fig. 3(a) shows a 3-electrode sensing circuit. When applying a DC sweeping voltage V_{appl} on the counter electrode (CE) to control the voltage V_w on the working electrode (WE), it will gradually break the equilibrium of the system and drive a redox reaction between the target molecules and the WE's material. The redox reaction generates electron transfer in the sweat and circuit, forming a current i_f from CE to WE, called *Faraday current*. During the voltage sweeping, a current peak will appear at a certain voltage. Then, we can obtain the current profile with the voltage sweeping and obtain the peak current. Mathematically, the peak current can be modeled as a function of the concentration of the target molecule [9]:

$$i_p = 0.4463(\frac{F^3}{RT})^{1/2} n^{3/2} A D_0^{1/2} C_0^* v^{1/2}, \quad (1)$$

where C_0^* is the concentration of the target molecule (in mol/cm^3), F is Faraday constant, the number of coulombs per mole of electrons ($F = 96485\ C/mol$), R is the universal gas constant ($R = 8.3\ J/K \cdot mol$), T is the temperature in kelvins, n is the number of transferred electrons to reduce/oxidize one target molecule, A is the area of the planar electrode (in cm^2), D_0 is diffusion coefficient (in cm^2/s), v is the applied voltage sweeping speed. In practice, the parameters F, R, T, n, D_0, v, A are constant. Therefore, the sensing peak current i_p is positively proportional to the target molecule concentration C_0^*. Thus, Eqn. (1) explains the sensing principle of UA/AA molecules.

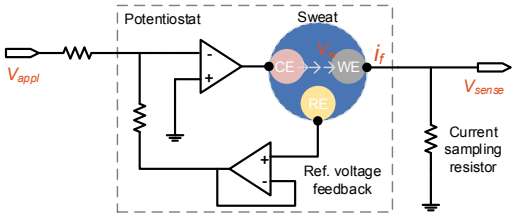

(a) The 3-electrode potentiostat circuit for sweat sensing.

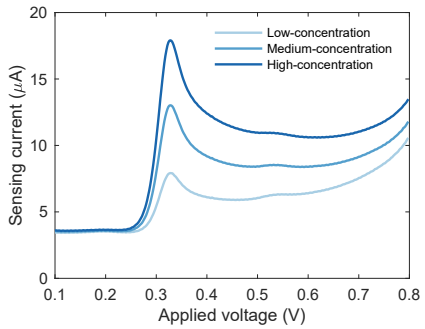

(b) The current-voltage features of different concentrations.

Figure 3: The basic sweat sensing circuit and the sensing feature. (a) shows the potentiostat circuit and the 3-electrode, which transduces the concentration of sweat into the current magnitude. (b) shows the measured current-voltage features of three concentration levels using the circuit in (a).

Fig. 3(b) shows the I-V profiles of three different UA concentrations in sweat. This figure verifies (i) the sensing current gradually rises to a peak and then declines with the applied voltage linearly varying; (ii) The peak current increases with the UA concentration increasing, which is used for sensing purposes.

Sensing Principle of Na^+ Ions. Different from molecule concentration sensing, the method for sensing Na^+ ions concentration is passive, which bypasses CE and just passively measures the potential difference between WE and RE. Furthermore, to only detect the concentration of Na^+ ions and avoid the interference of other ions, the working electrode is modified with the sodium selective membranes. Mathematically, the open circuit potential difference can be modeled by Nernst equation:

$$E = E^0 + \frac{RT}{nF} \ln(C_0^*), \quad (2)$$

where E^0 is the standard cell potential, and n is the valence of the ion and R, T, F are the same as Eqn. (1). For Na^+ ions, n is 1 and the other parameters E^0, R, T, F are constant. Thus, the potential difference E is directly related to the target ion concentration C_0^*. Hence, Eqn. (2) explains the sensing principle of Na^+ ions concentration.

3.2 Eliminating DAC for Low-Power Sweat Sensing

In order to capture the accurate I-V profile of the chemical reaction, the applied DC sweeping voltage should have high resolution, (i.e., fine-grained changes). To achieve this, the traditional proposal employs a digital-to-analog converter (DAC) to generate a fine-grained sweeping voltage that is applied to the potentiostat. However, the power consumption of DAC is high which accounts for nearly 60% power consumption of the micro-controller [52].

Basic idea. To eliminate the power-hungry DAC, our basic idea is that the voltage can be adjusted by continuously charging and discharging a capacitor of a passive RC circuit. Specifically, by controlling the duration of charging and discharging, the output voltage will change accordingly, which can be used as the applied sweeping voltage for the sweat sensor. To achieve voltage tuning, we exploit a pulse width modulation signal (PWM) based voltage sweeping circuit, which is comprised of a reconfigurable PWM signal and a second-order passive RC filter circuit, as shown in Fig. 4. The PWM signal is generated by a low-power micro-controller. In this way, we can greatly reduce the power consumption of the voltage sweeping function.

Challenge. Although the idea is straightforward, it is challenging in meeting the aforementioned two requirements for the sweat sensing application. Because the voltage sweeping resolution of the PWM-based solution is much lower than that of existing DACs. To analyze the resolution gap between DAC-based voltage sweeping and PWM-based voltage sweeping, we model the resolution of the two methods. The voltage resolution of the DAC-based method is:

$$Res_{dac} = \frac{V_{max}}{2^n - 1}, \tag{3}$$

where V_{max} represents the upper boundary of the applied sweeping voltage, n is the bit number of DAC, which means the DAC can divide V_{max} into $2^n - 1$ steps. The voltage resolution of the PWM-based method can be modeled as:

$$Res_{pwm} = \frac{V_{max} \cdot f_{pwm}}{f_{clk}}, \tag{4}$$

where f_{pwm} is the frequency of PWM signal, f_{clk} is the clock frequency of MCU. Thus, the PWM based method can divide the V_{max} into f_{clk}/f_{pwm} steps.

Now, let's use the following example to illustrate the challenge. Suppose that there is a 12-bit DAC and $V_{max} = 1V$. Then, DAC has a resolution of 0.2442 mV. For a PWM-based method, given f_{clk}=32.768 KHz and f_{pwm}=1 KHz, it has a resolution of 30.5 mV. It implies that *the voltage resolution of the PWM-based method is* 125× *lower than that of DAC*. Thus, the challenge question is: how can the PWM-based method achieve comparable performance as good as the DAC?

To improve the voltage sweeping resolution of the PWM-based method, a straightforward solution is to reduce the PWM signal frequency f_{pwm} or increase the clock frequency f_{clk} based on Eqn. (4). Note that, increasing f_{clk} would increase the power consumption of MCU. [1] Thus, the only way to increase the voltage sweeping resolution is to reduce the PWM signal frequency f_{pwm}.

[1] In this paper, we use the ultra-low power oscillator of MSP430 MCU with a clock frequency of 32.768 KHz.

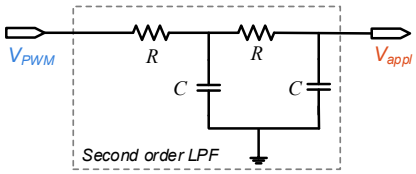

Figure 4: A pulse width modulation signal (PWM) based voltage tuning circuit. The PWM-based voltage tuning circuit replaces DAC to generate a sweeping voltage V_{appl} to the potentiostat and 3-electrode for sweat sensing. This circuit exploits the reconfigurable PWM signal from MCU and a passive lowpass filter.

However, it is challenging to reduce f_{pwm}, since a very low f_{pwm} would result in a large voltage fluctuation (i.e., ripple wave), leading to large sensing errors. Specifically, the fluctuation of the output voltage signal can be expressed as:

$$V_{ripple} = \frac{V_{max}}{4RCf_{pwm}}, \tag{5}$$

where V_{max} is the maximum voltage scale and V_{ripple} is the peak-peak value of the filtered PWM signal. As we can see, reducing f_{pwm} would increase V_{ripple} that characterizes the fluctuation of the output signal, which should be as low as possible.

Our solution. To combat the ripple wave output when f_{pwm} is low, our key observation is that *the charging voltage in the slow-rising phase is smooth and closer to the desired linear sweeping voltage waveform.* Thus, we can take advantage of the long rising time to emulate a linear voltage sweeping. Specifically, the rising stage is defined as settling time T_{settle}, which is a function of R, C, f_{pwm}:

$$T_{settle} = RC \cdot \ln(4RCf_{pwm}) \ . \tag{6}$$

From equations (5)(6), we find that *increasing R and C can not only extend the settling time but also reduce the ripple fluctuation.*

Based on this insight, we can solve the optimal $R,\ C,\ f_{pwm}$ to satisfy the key requirements of the circuit for sweat sensing. The requirements include the constraints of the DC signal's fluctuation frequency and amplitude for sensing fine-grained sweat changes, the voltage tuning speed for sensing sweat, and the current drain for reducing power consumption. We list all constraints about the three parameters $f_{pwm},\ R,\ C$ in the following.

(i) DC signal constraint:

$$f_{cutoff} = \frac{1}{2\pi RC}, \tag{7}$$

where f_{cutoff} is the cutoff frequency of the second-order RC low pass filter, which should be as low as possible to obtain a pure DC signal. We set f_{cutoff} less than 1 Hz, i.e.,

$$\frac{1}{2\pi RC} \leq 1.$$

(ii) Signal stability constraint:

$$\frac{V_{ripple}}{V_{max}} = \frac{1}{4RCf_{pwm}}, \tag{8}$$

To obtain a stable output, the ratio between the ripple voltage and the max voltage is set at less than 2^{-7}, i.e.,

$$\frac{1}{4RC \cdot f_{pwm}} \leq 2^{-7}.$$

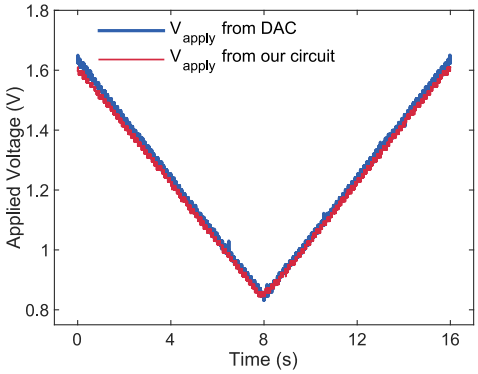

Figure 5: Comparison of DAC and our PWM-based voltage sweeping method. The optimized PWM-based voltage tuning circuit achieves a comparable resolution to a 12-bit DAC.

(iii) Slow-rising duration constraint: To achieve an approximate linear voltage sweeping, we set the rising time interval at 0.5 s–1 s, which can satisfy the flexible changing voltage sweeping speed for the sensing task. Thus, we have the following constraints:

$$0.5 \leq RC \cdot \ln(4RC \cdot f_{pwm}) \leq 1.$$

(iv) Current drain constraint: To reduce the power consumption, we use a large resistor to limit the current drain of the voltage sweeping circuit. We set the resistor at 1 MΩ, i.e.,

$$R = 10^6.$$

By solving the above inequalities and fine-tuning through simulation and the real test, we are able to find optimal values for f_{pwm}, R and C, i.e., 512 Hz, 1 MΩ and 0.1 μF for our BioScatter.

Verification through a real test. Based on the optimal values obtained, we demonstrate the effectiveness of our PWM-based voltage sweeping method by comparing its performance against a 12-bit DAC in MSP430MCU. Fig. 5 shows a comparison of the voltage sweeping, where we set the DAC and our PWM-based circuits to change their output voltage linearly and measure the output via an oscilloscope. As can be seen, the voltage sweeping of our PWM-based method is almost the same as the DAC-based method. Furthermore, in Sec. 5.1.1, we compare the sensing performance of the two methods. The results show that our PWM-based voltage sweeping method's performance is comparable to that of the DAC. These results imply that we can use our PWM-based voltage sweeping method for sweat sensing, thus eliminating the power-hungry DAC component.

3.3 Bypass ADC via Backscatter Communication

So far, we have built a sensing circuit that converts sweat concentration into voltage (or the I-V profile). Traditionally, one needs to first sample the I-V profile via an ADC and then transmit the sampled data to a remote reader [26, 56]. However, ADC components are usually energy-hungry, making the system unable to support continuous monitoring. To reduce the power consumption in the data transmission, we borrow the backscatter technology [25, 42, 45, 49] that can passively transmit the measured analog sensor values to the reader, thus avoiding high energy cost due to digital sampling.

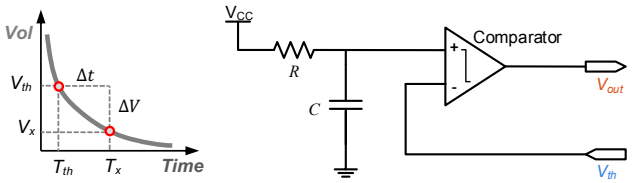

(a) The principle. (b) Supply voltage monitoring circuit.

Figure 6: Voltage monitoring principle and circuit. (a) shows the relationship between the capacitor voltage change and the discharging time. (b) BioScatter uses a capacitor, a comparator, and micro-controller to measure the supply voltage Vcc.

It is non-trivial to utilize backscatter in our system due to unstable backscatter energy harvesting [4, 18, 36, 39], making the supply voltage fluctuate and causing the sensing task to fail. To combat the supply voltage fluctuation, using a low-dropout (LDO) regulator is a common approach to supply a stable voltage [23]. However, the energy efficiency of LDO is usually low, since its key component (i.e. the regulator diode) would waste a lot of energy when bucking a high voltage to a low voltage.

To combat the supply voltage fluctuation and avoid energy waste, our key idea is to design a dynamic adjustment mechanism for the sensing circuit. Specifically, the micro-controller monitors the supply voltage in real-time and then calibrates the output of the PWM-based voltage sweeping circuit, which is the key to maintaining a desired sensing function. Such a design essentially adjusts the output voltage of the PWM-based voltage sweeping circuit according to the voltage demand of the subsequent circuit, rather than directly cutting the voltage from high to low, thus avoiding unnecessary energy waste. To monitor the voltage, we convert supply voltage changes into the capacitor's discharging time. To calibrate the output voltage of the PWM-based method, we increase the charging time (i.e., increasing the duty cycle of PWM) to allow more energy to be charged into the capacitor. Next, we illustrate the voltage monitoring and calibration method.

Voltage monitoring. Fig. 6(a) illustrates the basic principle of passive voltage measurement. Specifically, given a capacitor, the voltage decreases with time during the discharging period, which can be modeled by the following equation:

$$V_t = V_{full} \cdot e^{-\frac{t}{RC}}, \tag{9}$$

where V_t is the voltage of capacitor at time t, V_{full} is the voltage when the capacitor is full charged, R, C are the resistor and capacitor. If we set a threshold voltage V_{th} and measure the discharging time Δt from an unknown voltage V_x to V_{th}, we can derive the relationship between V_x and Δt as follows:

$$V_x = V_{th} \cdot e^{\frac{\Delta t}{RC}}. \tag{10}$$

As a result, we can monitor an unknown supply voltage by measuring the discharging time Δt. However, there is a practical issue in terms of the exponential calculation of Eqn. (10). Specifically, the exponential calculation of the micro-controller usually takes a relatively long time and thus incurs a delay in the practical system. Based on real tests on MSP430, the exponential calculation takes ~1 s, which however cannot achieve real-time voltage monitoring. To resolve this problem, we transform the exponential calculation

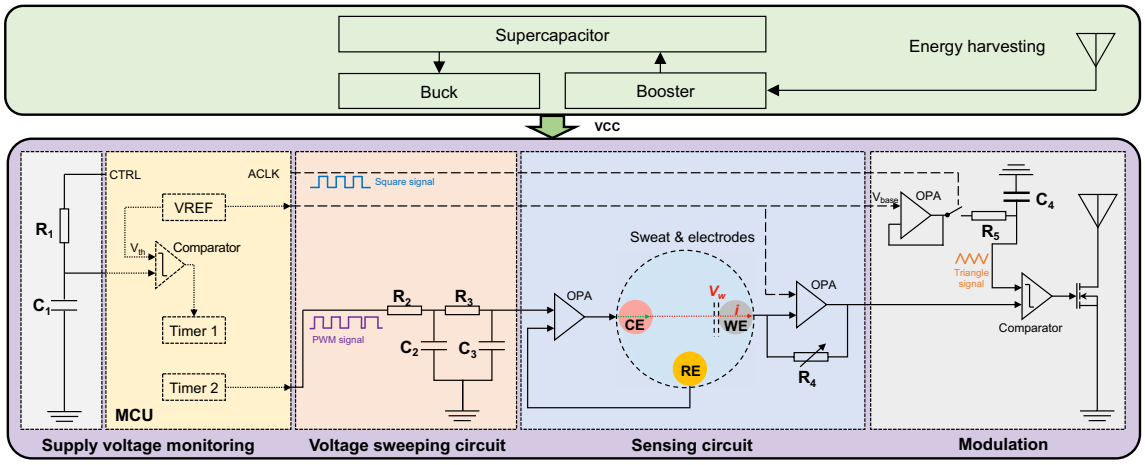

Figure 7: The schematic of the overall sweat sensing circuit.

into a table lookup operation, which reduces the delay to ~0.5 ms (i.e., 99.95% delay reduction than direct exponential computation).

Voltage calibration. After obtaining the supply voltage, we calibrate the output voltage by adjusting the duty cycle of the PWM signal. Under normal supply voltage V_{normal}, the desired voltage is proportional to the supply voltage, i.e., $V_{desired} = V_{normal} \cdot D$ where D is the duty cycle of the PWM signal. When the supply voltage fluctuates/changes from V_{normal} to V_x which is measured by Eqn. (10), the output of the voltage tuning circuit is not the desired voltage. To address this problem, we calibrate the duty cycle of the PWM signal by multiplying a coefficient, which is V_{normal}/V_x. Then, the calibrated output voltage is:

$$V_{desired} = V_{normal} \cdot D \cdot \frac{V_{normal}}{V_x}. \tag{11}$$

The calibration operation is conducted by the micro-controller every ~0.4 s which is approximate real-time. Therefore, the voltage monitoring and calibration can remove the impact of supply voltage fluctuation and output a correct voltage applied to the 3-electrode circuit for the sensing task. In Sec. 5.1.2, we evaluate the performance of voltage monitoring and calibration.

3.4 Putting All Together for Sweat Sensing

The whole circuit. By putting all the proposed modules together, we have the entire circuit as shown in Fig. 7. There are four modules:

- *Supply voltage calibration*: it combats the supply voltage fluctuation due to backscatter energy harvesting.
- *Sweeping voltage*: it provides the required sweeping voltage for sweat sensors without DAC.
- *Sweat sensing*: it is a widely used electrochemical-based sensing circuit with potentiostat and 3-electrode.
- *Backscatter modulation*: it transmits the sensing data to a remote reader via backscatter communication and eliminates the need for ADC.

In summary, the entire circuit realizes ultra-low-power sweat sensing by eliminating the power-intensive ADC, DAC, and active radios at the sensor side.

I-V profile extraction and concentration estimation. After the BioScatter tag transmits the sensing data to the reader by backscatter, the reader captures the tag's backscatter signal and demodulates the I-V profile. Specifically, by using Short-Time Fourier Transformation (STFT) on backscatter signals, we can extract the power of the direct current (DC) component in the time domain which is the desired I-V profile. To estimate the sweat concentration, we first measure I-V profiles of different concentrations and then extract the peak current of each concentration. The multiple peak current values can be fitted to a linear function of concentration levels, which is used for the sweat concentration estimation.

4 IMPLEMENTATION

We have designed, fabricated, and implemented BioScatter using commodity components and materials, as illustrated in Fig. 8.

BioScatter Tag. We implement BioScatter on flexible PI substrates which is a four-layer PCB. The tag consists of five parts: the microcontroller, the sensing circuit, the sensor electrodes, the energy management unit, and the backscatter communication.

(i) The MSP430FR2355 is selected as the MCU. We set a low clock frequency (32.768 KHz) for its external crystal oscillator to achieve low power consumption. Note that we don't use the MCU's internal DAC for our sensing purpose.

(ii) The sensing circuit is implemented using commodity passive electronics such as amplifiers, resistors, and capacitors. Specifically, we employ an ultra-low-power operation amplifier LPV802 to reduce power consumption. The voltage monitoring comprises a capacitor of 0.1 μF and a resistor of 400 KΩ. The charging duration is set at 0.4 s, which is 10 times of RC constant, i.e., $10 \cdot RC$.

(iii) The sensor electrodes are implemented using screen printing technology. For molecular substance detection (i.e., urea acid and ascorbic acid), the 3-electrode patch is employed as shown in Fig. 9 (a). The material of the working electrode is carbon fabric, the counter electrode is carbon ink, and the reference electrode is Ag/AgCl. Note that the measured current/voltage value is also related to the working electrode's area. Thus, we set the area of the working electrode in all experiments at 1 cm^2. For Na^+ ion detection, the sensor only needs the working electrode and the

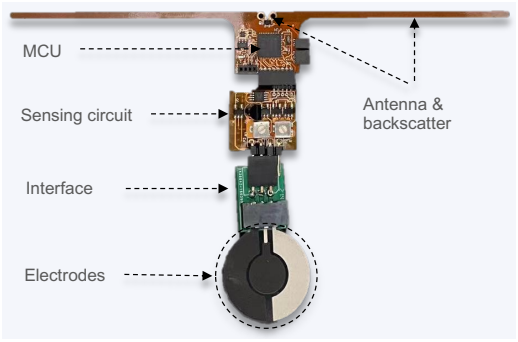

Figure 8: The fabricated BioScatter tag. The tag is a four-layer PCB made with a flexible PI substrate, which is comprised of a micro-controller, a sensing circuit, an interface for connecting the circuit and electrodes, and an antenna for communication.

reference electrode, as shown in Fig. 9 (b). To selectively detect Na^+ concentration in sweat, we add sodium ion-selective membranes on the carbon fabric to make the working electrode, and the reference electrode's material is Ag/AgCl.

(*iv*) The energy management circuit consists of an energy harvest module, a supercapacitor as an energy buffer, and a voltage booster and bucker. The booster and bucker is a commercial chip BQ25570. The charging and discharging threshold are set at 1.8 V, which is the minimum voltage required by MCU.

(*v*) The backscatter communication should satisfy two design requirements – low power and robustness to self-interference, mobility, and multipath interference. We evaluate three types of circuits including (*i*) frequency modulation with a commodity voltage-controlled oscillator (VCO) [45], (*ii*) frequency modulation with a customized VCO circuit, and (*iii*) a customized pulse width modulation circuit [42]. By evaluating their performance and power consumption, we find that the three circuits have the same performance while analog pulse width modulation has the lowest current drain. Thus, we finally decide to employ pulse width modulation. Then, the resultant baseband signal controls a MOSFET to switch between reflective and absorbing states to realize backscatter communication.

Reader. We implement a reader with USRP N210 and UBX40 daughterboard and control it with a laptop. We set the center frequency of USRP at 910 MHz and add a continuous sine wave with a frequency of 500 KHz as the payload. The sampling rate of USRP's receive chain is 5 MHz. The backscatter signal demodulation and the concentration estimation are implemented by MATLAB.

5 EVALUATION

In this section, we first conduct benchmark experiments to evaluate our PWM-based voltage sweeping circuit and the voltage monitoring and calibration circuit. Then, we conduct experiments to understand the sensing performance of BioScatter, followed by an overall sensing accuracy evaluation. Next, we evaluate the backscatter communication performance, followed by a case study to show the feasibility of continuous sweat monitoring. Lastly, we evaluate the power consumption of BioScatter.

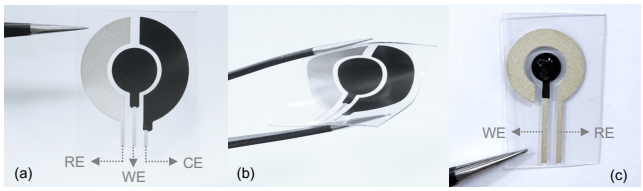

Figure 9: The fabricated sensing electrodes. (a) shows the electrode patch for sensing UA/AA. (b) shows the bending electrode patch. (c) shows the electrode patch for selectively sensing Na^+ ions where the working electrode is the middle circle, modified with the sodium selective membrane, and the outer circle is Ag/AgCl reference electrode.

5.1 Benchmark Experiments

5.1.1 Comparison of voltage sweeping on sensing performance with our PWM-based circuit and DAC. To compare the performance, we measure the sensing currents (i.e., I-V profiles) of urea acid (UA) and ascorbic acid (AA) when using the two methods, i.e., DAC-based voltage sweeping and our PWM-based voltage sweeping methods.

Fig. 10(a) and Fig. 11(a) show the I-V profiles for UA and AA with the same concentration level (40 $\mu mol/L$). We sweep the voltage from 0 V to 0.8 V and then back to 0 V, which is the so-called cyclic voltammetry. The forward direction (0⟶0.8) can obtain the I-V profile of the oxidation reaction, while the reverse direction (0.8⟶0) can obtain the I-V profile of the reduction reaction. [2] As we can see, the I-V profiles measured by our PWM-based circuit are close to the ones measured by DAC, i.e., they have the same profile shape and the same peak current. Although there are some non-overlapping parts, the differences are small and do not affect the sensing accuracy. Fig. 10(b) and Fig. 11(b) show correlations of two I-V profiles measured by our PWM-based circuit and DAC for UA and AA, respectively. The correlations are more than 95% for both UA and AA, demonstrating that our PWM-based method can achieve the same sensing performance as the DAC-based method.

5.1.2 Performance of Voltage Monitoring and Calibration. Voltage monitoring and calibration are the key components to combat supply voltage fluctuation. Therefore, in this experiment, we evaluate the accuracy of our voltage monitoring and calibration method. Specifically, we generate a supply voltage that varies from 1.8 V–3.3 V at an interval of 0.1 V. At each voltage, we use our voltage monitoring circuit to measure it 10 times. Fig. 12 shows the voltage monitoring results, where the red line is the ground truth and the gray dots are the measured voltage by our circuit. We can see that the measured values are very close to the ground truth. The mean error is only 2.7 mV and the largest error is < 10 mV. The results demonstrate that our voltage monitoring method can provide accurate feedback for the voltage sweeping circuit.

Further, we show voltage calibration results in Fig. 13 where the blue line is the sweeping voltage that is affected by the fluctuated supply voltage and the black dash line is the ideal one. We observed that the sweeping voltage without our calibration method suffers larger errors due to the supply voltage fluctuation. While, by using our voltage calibration method, we can combat the supply voltage

[2] In electrochemical detection, the substances are divided into oxidation type and reduction type depending on their intrinsic chemical properties.

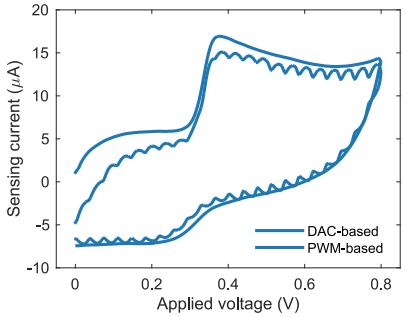

(a) I-V profile comparison.

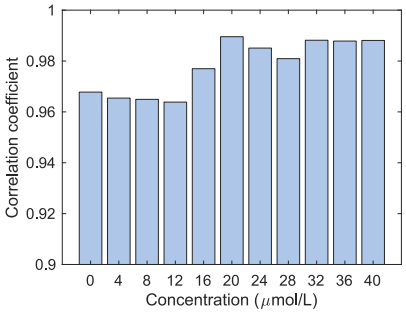

(b) The I-V profile's correlation.

Figure 10: The performance comparison of sensing urea acid (UA).

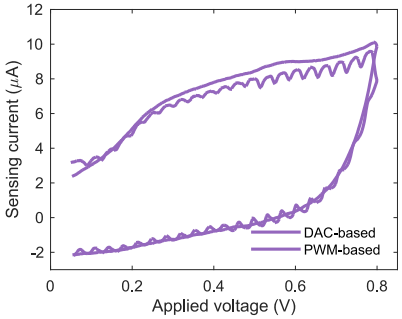

(a) I-V profile comparison.

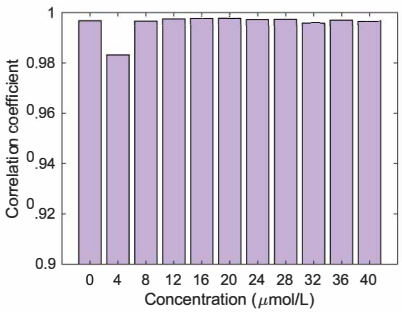

(b) The I-V profile's correlation.

Figure 11: The performance comparison of sensing ascorbic acid (AA).

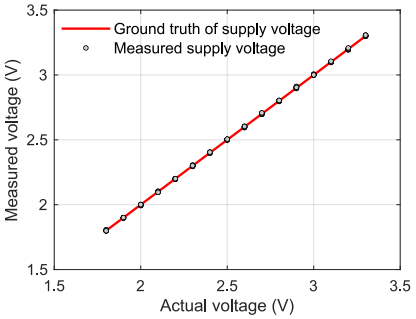

Figure 12: Voltage monitoring accuracy.

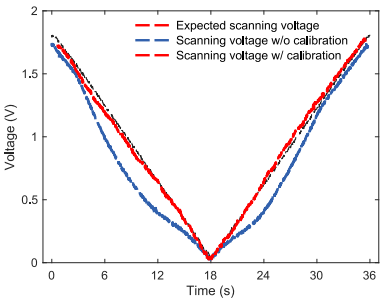

Figure 13: Sweeping voltage calibration.

fluctuation and provide sweat sensors with a sweeping voltage that is close to the ideal one.

5.2 Understand The Sensing Performance

We conduct experiments to understand the sensing performance of BioScatter on urea acid (UA), ascorbic acid (AA) and Na^+. Specifically, we examine the sensitivity and stability of the sensing circuit by conducting 10 groups of experiments for each substance. The **sensitivity** indicates how finer concentration can be sensed, which is defined as $\Delta I/\Delta C$, i.e., the ratio between the change in sensing current ΔI and the change in the substance's concentration ΔC. The **stability** indicates the consistency of measurement results for the same concentration level, which can be calculated as the standard deviation of multiple measurements' bias.

5.2.1 Sensing Urea Acid (UA). For urea acid (UA), we test 11 concentration levels, from 0 $\mu mol/L$ to 40 $\mu mol/L$ with a step of 4 $\mu mol/L$. We set the concentration range of 0–40 $\mu mol/L$ because the normal urea acid concentration in human sweat is 20–30 $\mu mol/L$ [27]. In this experiment, we use artificial sweat to simulate human sweat. [3] Specifically, we first prepare a urea acid solution with a high concentration of 3 $mmol/L$. Then, we take 15 mL artificial sweat as the base solution and put 20 μL high concentration UA solution into the artificial sweat, finally obtaining the sweat that contains a 4 $\mu mol/L$ urea acid. Every time adding 20 μL of the high-concentration UA solution, the concentration increases by 4 $\mu mol/L$.

Fig. 14(a) shows the measured I-V profiles of different concentrations at 8 $\mu mol/L$ interval for clarity. It shows that the peak current happens when the applied voltage is 0.36 V. It implies that the voltage sweeping range can be set at 0.2–0.5 V for getting the peak current, which is a robust sweat sensing feature [7]. Fig. 14(b) shows the peak current of different concentrations, where the black dots are measured values of 10 groups and the red line is the fitted curve. As we can see, there is a strong linear relationship between the peak sensing current and the UA concentration, and the goodness-of-fit is $R^2 = 0.95$, demonstrating good linearity. Based on the linear curve, we can calculate the sensitivity that is 0.5 $\mu A/\mu molL^{-1}$. We also evaluate the stability/bias of our sensing circuit. Fig. 14(c) shows the probability distribution of all concentrations' biases. We can see that the 90% biases are within ±3 μA, demonstrating good stability.

5.2.2 Sensing Ascorbic Acid (AA). To understand the sensing performance of AA, we test 11 concentration levels from 0 $\mu mol/L$ to 40 $\mu mol/L$ at a step of 4 $\mu mol/L$. The tested process is the same as that of urea acid. Fig. 15(a) shows the measured I-V profiles of different concentrations at 8 $\mu mol/L$ interval for clarity. It shows that the peak position is 0.41 V, indicating that the voltage sweeping range can be set at 0.3–0.6 V for sensing AA. Fig. 15(b) shows the peak current of different AA concentrations, where the black dots are measured values of 10 groups and the red line is the fitted curve. As we can see, there is also a strong linear relationship between the peak sensing current and the AA concentration, and the goodness-of-fit is $R^2 = 0.958$, demonstrating good linearity. Based on the linear curve, we can calculate the sensitivity that is 0.45 $\mu A/\mu molL^{-1}$. Fig. 15(c) shows the bias distribution of AA sensing current. As we can see, the 90% biases are within -4 ~ +2 μA, demonstrating good stability.

[3] The artificial sweat includes NaCl, urea, lactic acid, and 98% water.

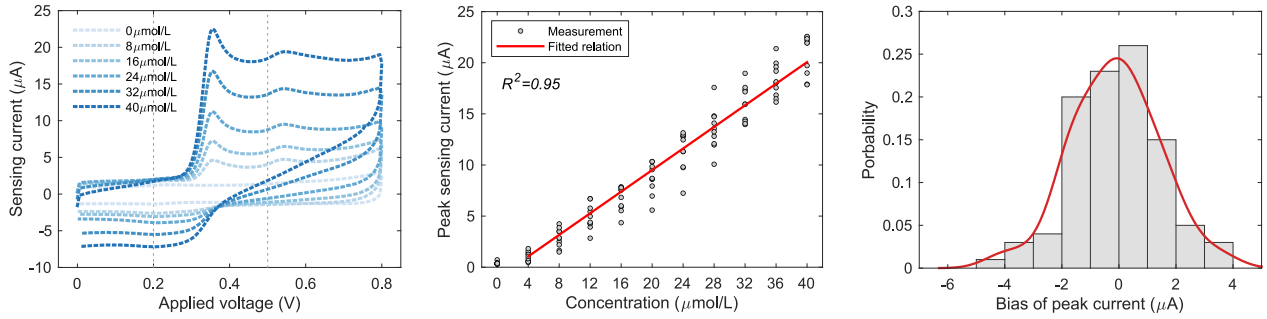

(a) I-V profiles of sensing UA. (b) Peak sensing current vs. UA concentration. (c) The bias distribution of our sensor.

Figure 14: I-V profiles of sensing urea acid (UA) and our sensor's performance in sensitivity and stability.

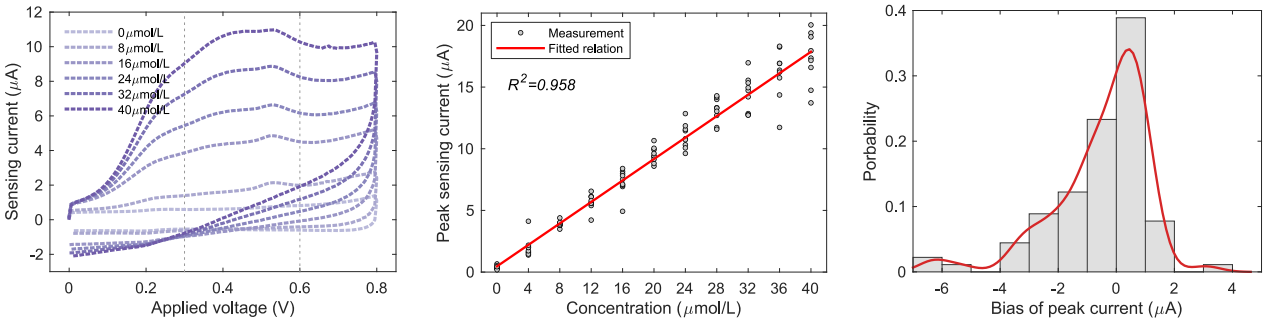

(a) I-V profiles of sensing AA. (b) Peak sensing current vs. AA concentration. (c) The bias distribution of our sensor.

Figure 15: I-V profiles of sensing ascorbic acid (AA) and our sensor's performance in sensitivity and stability.

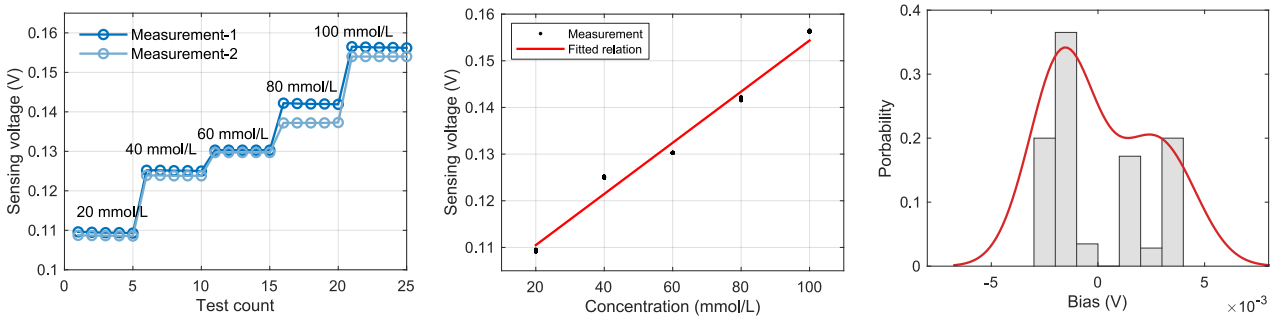

(a) The voltage profile of sensing Na^+. (b) Sensing voltage vs. Na^+ concentration. (c) The bias distribution of our sensor.

Figure 16: The voltage profile of sensing Na^+ ion and our sensor's performance in sensitivity and stability.

5.2.3 Sensing Na^+ ion. By measuring the voltage difference between WE and RE electrodes shown in Fig. 3(a), we can sense the Na^+ concentration in sweat. The working electrode material is the carbon fabric coated with the Na^+ selective membrane. We test five Na^+ concentration levels from 20 $mmol/L$ to 100 $mmol/L$ with a step of 20 $mmol/L$. At each level, we obtain five sensing voltage values. We select the test range of 20–100 $mmol/L$ because the normal Na^+ concentration in sweat is 42–88 $mmol/L$ [14]. We repeat the test twice using the same setup and obtain the sensing profiles of measurement-1 and measurement-2. Fig. 16(a) plots the sensing voltage profiles of different Na^+ concentrations. The test count is the measurement times. As expected, the sensing voltage grows from 0.11 V to 0.157 V with the concentration increasing. In addition, the two profiles have a slight difference in 80 $mmol/L$ and 100 $mmol/L$. This is because the amount of absorbed Na^+ selective membrane solution by two working electrode materials has a slight difference, which is a common experimental error and can be removed by repeating the measurement many times. Fig. 16(b) shows the relationship between the measured voltage and the Na^+ concentration, where each black dot means one measurement and the red line is the fitted linear curve. The goodness-of-fit is $R^2 = 0.97$, demonstrating good linearity. The sensitivity is $10mV/20mmolL^{-1}$. Fig. 16(c) shows the bias of sensing voltage among all tests. As we can see, the 90% bias of sensing voltage is within -3 mV–4 mV, showing good stability.

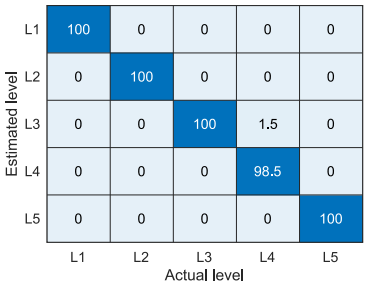

Figure 17: The accuracy of sensing urea acid (UA).

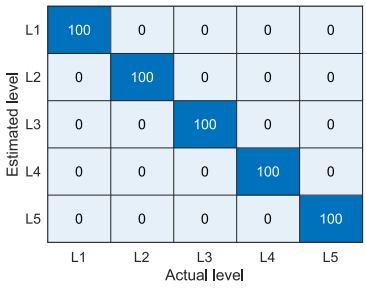

Figure 18: The accuracy of sensing ascorbic acid (AA).

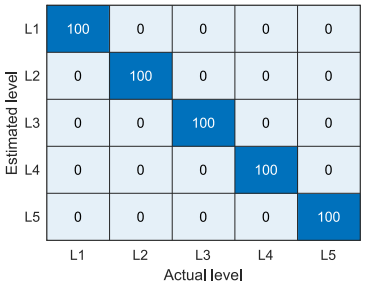

Figure 19: The accuracy of sensing Na^+ ions.

5.3 Overall Sensing Accuracy

We evaluate the overall sensing accuracy of BioScatter on detecting five concentration levels of urea acid (UA), ascorbic acid (AA), and Na^+. The five levels are shown in Table. 2. Note that the five levels are good enough to meet the requirement of medical since hospitals usually only need a three-level detection (i.e., normal level, below the normal level, and higher than normal level).

Table 2: Concentration levels for testing accuracy.

	L1	L2	L3	L4	L5
UA concentration (in $\mu mol/L$)	0–8	8–16	16–24	24–32	32–40
AA concentration (in $\mu mol/L$)	0–8	8–16	16–24	24–32	32–40
Na^+ concentration (in $mmol/L$)	0–20	20–40	40–60	60–80	80–100

The accuracy of sensing UA in a mixture of artificial sweat. In this experiment, the tested solution is made with artificial sweat and the urea acid solution. The concentration of urea acid ranges from 0 $\mu mol/L$ to 40 $\mu mol/L$ at a step of 8 $\mu mol/L$. Specifically, we first prepare the artificial sweat with PH=5.5 and an aqueous solution of UA with a high concentration of 3 $mmol/L$ using UA reagent and deionized water, then take the artificial sweat 15 mL and the UA aqueous solution 40 μL and mix them, and finally obtain the concentration of artificial sweat with the concentration of 8 $\mu mol/L$. [4] The tag-to-reader distance is set at 2 m. At the reader side, we capture the backscatter signal, demodulate I-V profiles, and estimate the concentration. For each concentration level, we conduct 200 estimations, and the results are shown in Fig. 17. As we can see, the sensing accuracy for UA is more than 98.5% when detecting the five concentration levels in the range of 0–40 $\mu mol/L$, i.e., BioScatter has a sensing resolution of 8 $\mu mol/L$.

The accuracy of sensing AA in a mixture of artificial sweat. For evaluating the sensing accuracy of AA, the experimental setup and the tested solution preparation process are the same as that of UA. Fig. 18 shows the sensing accuracy of the five concentration levels. We can see that the sensing accuracy is 100% when detecting five concentration levels in the range of 0–40 $\mu mol/L$, i.e., achieving a sensing resolution of 8 $\mu mol/L$ for AA.

From the two experiments, we have two more observations: 1) As the concentration of UA/AA increases, the rate of increase in sensing current slows down. Therefore, in high concentration levels, the sensing results are more susceptible to experimental errors, which can reduce the accuracy of the sensing. To achieve greater accuracy in high concentration levels, we conducted 100 tests for both UA and AA, which led to improved sensing accuracy. 2) In principle, the IV profiles of UA and AA have different peak locations and are used to distinguish between them. However, in practice, the IV profile of a mixture solution of UA and AA does not display distinguishable peaks due to imperfections in the electrode material. This issue can be addressed by using differential pulse voltammetry, which leaves for our future works.

The accuracy of sensing Na^+. Following the same setup of testing UA and AA, we conduct experiments to evaluate the Na^+ sensing accuracy. For each concentration level, we conduct 100 estimations, and the results are shown in Fig. 19. As we can see, BioScatter achieves 100% sensing accuracy when identifying the five concentration levels in the range of 20–100 $mmol/L$, i.e., BioScatter has a sensing resolution of 20 $mmol/L$. Such good performance is attributed to the selective permeability of sodium ion-selective membrane to sodium ion and the good conductivity of carbon cloth. In this experiment, it is noted that the ion-selective material gradually dissolves into the sweat, resulting in a reduction in the amount of the ion-selective material. Therefore, as the number of measurements increases, the sensing voltage is lower than the true voltage. This means that the electrode patches should be replaced frequently in actual use to ensure the most accurate sensing result.

5.4 Impact of Distance and User's Movement

BioScatter employs backscatter communication to bypass the energy-hungry ADC component. Thus, the quality of the backscatter signal is important for the sensing accuracy, e.g., a poor backscatter signal may cause the demodulation of sensing data to fail. To this end, we evaluate the Signal-to-Noise Ratio (SNR) of both the received backscatter signal and the demodulated baseband signal under different working ranges and the user's movement.

5.4.1 Impact of distance. We examine SNR changes over different tag-to-reader distances. To do so, we use a *sin* wave as the analog baseband signal to emulate the I-V profiles of sweat sensing. We vary the tag-to-reader distance from 0.6 m to 21 m at a step size of 1.2 m. The transmit power is set at 25 dBm.

Fig. 20 shows the SNR of both the received backscatter signal and the demodulated baseband signal under different working ranges. As we can see, even with a 21 m long distance, SNR values of both backscatter signals and demodulated signals are very high, i.e., around 8.64 dB and 26.5 dB, respectively. Note that, almost all RF transceivers can receive signals that have SNR < 0, e.g., the receive

[4] The actual human sweat PH is 4.5–7.0.

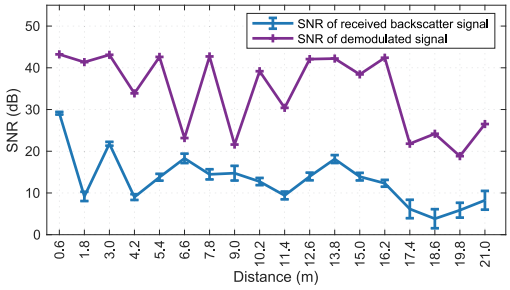

Figure 20: SNR vs. Distance.

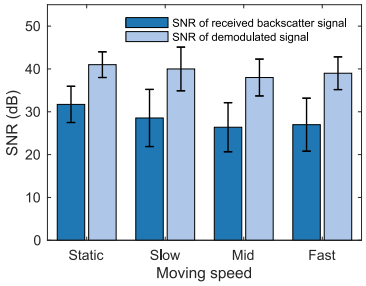

Figure 21: SNR vs. Moving speed.

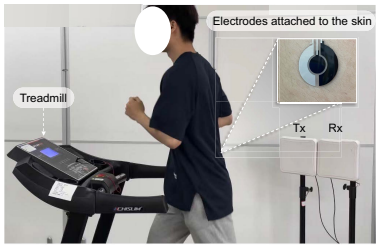

Figure 22: The setup of in vitro experiment.

sensitivity of commodity Wi-Fi devices is around -60 dB. Thus, this experiment implies that our BioScatter can work at 21 m.

5.4.2 Impact of user's movement. To create a dynamic environment, we mount our BioScatter tag on a person's arm and ask the person to move around in an indoor environment. There are four kinds of moving speed, i.e., the static state, the slow movement of 4-5 km/h, the medium movement of 7-8 km/h, and the fast movement of 9-10 km/h. For each movement speed, we measure the SNR of the received backscatter signals and the demodulated signals. The results are shown in Fig. 21. Compared to the static state, the mean SNR of demodulated signals in slow, medium, and fast speeds decreases by only 2.2 dB, 5.4 dB, and 4.8 dB. It implies that the movement and the environment noise do not have a great impact on BioScatter's signal quality.

Furthermore, we also observed that the body's dramatic movement will cause the electrodes to not fit tightly to the skin, thus affecting the sensing results. To avoid this impact, one can employ a more flexible material such as PDMS and hydrogel as the substrate of electrodes.

5.5 Case Study

Finally, we conduct a case study to evaluate the performance of continuously monitoring the total concentration of urea acid and ascorbic acid in a person's skin sweat when he running on a treadmill. Specifically, we ask a volunteer to run on a treadmill and test his sweat's I-V profile during his running. We put a 3-electrode sensor patch on his lower back, where the sweating rate is higher, and measure the I-V profile every minute. The experiment setup is shown in Fig. 22.

Fig. 23 shows the urea acid and ascorbic acid concentration changes during the user is running on a treadmill. In the first four minutes, the user warmed up at a speed of 5 km/h, and therefore, there was no noticeable sweating during this period. As shown in Fig. 23, the measurement result for the first five minutes was 0. From the 5th minute to the 18th minute, the user ran at a speed of 8 km/h. During this period, the user gradually started to sweat, but the amount of sweat was relatively low between 5-15 minutes. The concentration shown in Fig. 23 fluctuated around 1 $\mu mol/L$. At the 15th minute, the amount of sweat began to increase, and it reached 3.3 $\mu mol/L$ at the 18th minute. At the 19th minute, the user stopped for one minute to rest, resulting in some evaporation of the sweat and a decrease in the measured concentration. From the 20th minute to the 27th minute, the user continued to run at a speed of 8 km/h. During this period, the user's body temperature

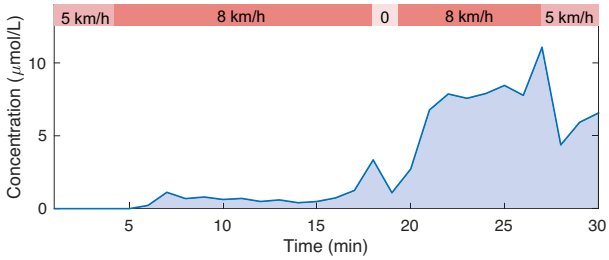

Figure 23: The sweat concentration changes in sweat.

increased sharply, leading to an increase in the sweat rate, and thus the measured concentration reached 11 $\mu mol/L$. After 27 minutes, the user began to walk at a speed of 5 km/h and finished running at the 30th minute. Therefore, the concentration at the 28th minute decreased slightly and then remained around 6 $\mu mol/L$.

In this experiment, there are two points to be noted: 1) As mentioned before, when the user is running, the electrodes do not fit tightly to the skin since the PET substrate is not flexible enough. In future works, we will improve this issue by using PDMS or hydrogel as the substrate. 2) When the skin has no apparent sweat, the sensing result is zero since three electrodes need to be in the same sweat solution to form a current path. In future works, we will employ a microfluidic channel to capture micro sweat drops.

5.6 Power Consumption

BioScatter aims to achieve low-power sweat sensing. Thus, we evaluate the power consumption of BioScatter tag. Specifically, we measure the power consumption of every single module in BioScatter tag and then add them together. Specifically, we use the TI MSPFET hardware programming tool with EnergyTrace technology [53] to evaluate the average power consumption of MCU. For analog circuits, we measure the current drains from the Vcc pin when the module is working. Then, the power consumption equals the Vcc times the current. Table. 3 shows the power consumption of our BioScatter and other related systems. As we can see, Apollo reduces the power consumption of the sweat sensor tag from ~200 mW to 23.88 mW, achieving a ~90% reduction compared to traditional active radios-based sensor tags. While BioScatter pushes the power consumption of the sweat sensor tag to only 313.5 μW. Compared

Table 3: Power consumption.

Systems	MCU	ADC/DAC	Osc.	Sensor	Comm.	Total
NutriTrek [56]	39.6 mW			122.1 mW	39.6 mW	201.3 mW
Apollo [59]	10.11 mW	7.2 mW	0.59 mW	5.8 mW	0.18 mW	23.88 mW
Our BioScatter	105.6 μW	0 μW	3.3 μW	105.6 μW	99 μW	313.5 μW

with the SOTA backscatter-based sensing system 'Apollo', BioScatter reduces the power consumption by 98.69%.

6 RELATED WORK

Commercial sweat sensing devices. Electrochemical workstations [7, 29] are commercial analytical tools for sensing sweat concentration, providing high sensitivity in analyzing the chemical reaction property and detecting trace amounts of substances. However, they are bulky, expensive, and have high power consumption, making them unsuitable for low-power and compact wearable devices/applications. To reduce the sensing system's size, many studies [5, 13, 17, 35] design miniaturized measurement circuits for portable devices. However, they still rely on the energy-hungry DAC and ADC for controlling the applied voltage and sampling the measured sensor values. Other studies [16, 22] employ a low-power electrochemical gas detection chip to build wireless and simple portable sensors. However, this chip can only provide a coarse I-V profile [13, 51], leading to limited sensing accuracy.

Compared to the above studies, our system realizes an ultra-low power and accurate electrochemical-based sweat sensor, without the need for energy-hungry DAC and ADC. Moreover, our swear sensor has a small form factor due to the use of commodity passive components and flexible materials.

Wearable sensing devices. Wearable devices aim to wirelessly and long-term monitor body information, such as heart rate and steps. They usually employ Wi-Fi or Bluetooth [57] to wirelessly transmit the sensing data to the mobile device (e.g., smartphone). However, due to the use of active Wi-Fi/BLE radios, the communication energy cost of those wearable devices is high. To reduce the communication energy cost, some researchers employ passive Near Field Communication (NFC) [8, 38, 43]. However, the working range of NFC usually is no more than 10 cm, which limits real-world applications. Recently, Yuan *et al.* [59] proposed a wearable sweat sensor tag (named Apollo), which combines a biochemical sensor array and a low-power Bluetooth backscatter. Apollo tag can send data to a commercial BLE device and achieve a longer distance than NFC, offering the possibility for mobile wearable sensing applications. However, the power consumption of this wearable sensor is still relatively high, i.e., 23.88 mW. In contrast, BioScatter exploits analog backscatter as the uplink modulator to modulate the analog sensing information into the time domain of the backscatter signal, thus avoiding the need for ADC for sensing information digitization. The total power consumption of BioScatter tag (including sensing and communication) is only 313.5 μW, making it an ultra-low-power and accurate electrochemical-based sweat sensor that is suitable for wearable devices.

Energy harvesting and management. Many works adopt an integrated boost and buck circuit (e.g., BQ25570 chip) and low-dropout regulator (LDO) for energy management [45, 54, 58, 59]. They usually focus on sustaining a regular and constant working voltage (e.g., 3.3 V). In contrast, BioScatter can adapt to intermittent energy harvesting situations by dynamic voltage monitoring and calibration. This benefits from the proposed novel hardware design, i.e., the low-power 3-electrode electrochemical measurement circuit, and the real-time voltage monitoring/calibration mechanism. Owing to these designs, BioScatter fulfills the low-power and mobile biochemical sensing applications.

7 DISCUSSION AND FUTURE WORKS

Limitations. While the preliminary results are promising, the current implementation of BioScatter has the following limitations. First, the electrode design is not suitable for small amounts of sweat and can detect the concentration of one substance of each electrode in sweat. To detect different substances, we need to replace the electrodes manually. Second, the detected substances are only three substances, i.e., urea acid, ascorbic acid, and Na^+ ion. Other substances in sweat are also crucial for evaluating health conditions, such as urea molecule [40], cortisol [55], and K^+ ion [37]. Third, when the supply voltage fluctuates dramatically, the calibration may not output a correct voltage to the electrodes. Fortunately, dramatic voltage fluctuation rarely happens in real applications since the supply power is stored in a supercapacitor. The charging and discharging processes are usually slow due to low energy harvesting efficiency and power consumption.

Future works. In the future, we will improve the design of the sweat collection method to adapt to small amounts of sweat by developing microfluidic channels [15, 34] to collect the sweat drop for more precise sensing. In addition, we will develop multichannel electrodes which get rid of manually replacing the electrode. Further, we will optimize the circuit design to support more substance sensing such as urea molecule, cortisol, and K^+ ion. In particular, we will develop new electrode materials that can selectively produce the reduction/oxidation reaction with the urea molecule and cortisol. For K^+ ion, we will use the K^+ ion-selective membranes to modify the electrode. To achieve high-duty-cycled sweat sensing in the long-term application, we will explore a more reliable energy harvesting system with multiple energy sources, such as TENG [32], and heat energy [31, 41, 48].

8 CONCLUSION

This paper proposed a backscatter-based ultra-low-power sweat sensing wearable sensor. By designing a novel low-power voltage sweeping circuit, which can perform as well as a 12-bit DAC, we can eliminate the energy-hungry DAC in sweat sensing circuits. By utilizing the backscatter technology, our sweat sensor can directly transmit the measured analog sensing values to the reader, thus avoiding the need for ADC for digital sampling. We also designed a fully passive supply voltage monitoring and calibration circuit to combat supply voltage fluctuation due to unstable energy harvesting. We believe our design can benefit other bio-sensors for achieving low-power sensing without the need for DAC, ADC, and active radios.

ACKNOWLEDGMENTS

This work is supported by the National Natural Science Foundation of China under Grants (62172332, 62272388), the NSFC A3 Foresight Program under Grant 62061146001, and the Shaanxi International Science and Technology Cooperation Program under Grant 2023-GHZD-06. We thank Prof. Sheng Tang and Prof. Fengchun Yang for their valuable comments. We also thank anonymous reviewers and the shepherd for their valuable feedback.

A APPENDIX

The research artifact accompanying this paper is available via https://doi.org/10.5281/zenodo.7922850.

REFERENCES

[1] Impact of ux on wearables and iot, 2016. https://suyati.com/blog/impact-of-ux-on-wearables-and-iot/.

[2] Extending the battery life of electronic wearable devices, 2017. https://www.volersystems.com/blog/extending-the-battery-life-of-electronic-wearable-devices.

[3] Overview of wearable device sensors, 2017. https://www.volersystems.com/blog/news/overview-wearable-device-sensors-slides-2017.

[4] Mikhail Afanasov, Naveed Anwar Bhatti, Dennis Campagna, Giacomo Caslini, Fabio Massimo Centonze, Koustabh Dolui, Andrea Maioli, Erica Barone, Muhammad Hamad Alizai, Junaid Haroon Siddiqui, et al. Battery-less zero-maintenance embedded sensing at the mithræum of circus maximus. In *Proceedings of the 18th Conference on Embedded Networked Sensor Systems*, pages 368–381, 2020.

[5] Alar Ainla, Maral PS Mousavi, Maria-Nefeli Tsaloglou, Julia Redston, Jeffrey G Bell, M Teresa Fernandez-Abedul, and George M Whitesides. Open-source potentiostat for wireless electrochemical detection with smartphones. *Analytical chemistry*, 90(10):6240–6246, 2018.

[6] Apple. Apple watch, 2022. https://www.apple.com.cn/apple-watch-series-8/.

[7] Eric Bakker and Martin Telting-Diaz. Electrochemical sensors. *Analytical chemistry*, 74(12):2781–2800, 2002.

[8] Amay J Bandodkar, Philipp Gutruf, Jungil Choi, KunHyuck Lee, Yurina Sekine, Jonathan T Reeder, William J Jeang, Alexander J Aranyosi, Stephen P Lee, Jeffrey B Model, et al. Battery-free, skin-interfaced microfluidic/electronic systems for simultaneous electrochemical, colorimetric, and volumetric analysis of sweat. *Science Advances*, 5(1):eaav3294, 2019.

[9] Allen J Bard, Larry R Faulkner, and Henry S White. *Electrochemical methods: fundamentals and applications*. John Wiley & Sons, 2022.

[10] M. Bariya, Hyy Nyein, and A. Javey. Wearable sweat sensors. *Nature Electronics*, 1(3):160–171, 2018.

[11] Ahmet Baskan and Gozde Goncu-Berk. User experience of wearable technologies: A comparative analysis of textile-based and accessory-based wearable products. *Applied Sciences*, 12(21):11154, 2022.

[12] Vidula Bhole, Jee Woong J Choi, Sung Woo Kim, Mary De Vera, and Hyon Choi. Serum uric acid levels and the risk of type 2 diabetes: a prospective study. *The American journal of medicine*, 123(10):957–961, 2010.

[13] Valentina Bianchi, Andrea Boni, Simone Fortunati, Marco Giannetto, Maria Careri, and Ilaria De Munari. A wi-fi cloud-based portable potentiostat for electrochemical biosensors. *IEEE Transactions on Instrumentation and Measurement*, 69(6):3232–3240, 2019.

[14] Michael J. Buono, Kimberly D. Ball, and Fred W. Kolkhorst. Sodium ion concentration vs. sweat rate relationship in humans. *Journal of Applied Physiology*, 103(3):990–994, 2007.

[15] Jungil Choi, Roozbeh Ghaffari, Lindsay B Baker, and John A Rogers. Skin-interfaced systems for sweat collection and analytics. *Science advances*, 4(2):eaar3921, 2018.

[16] Andres Felipe Diaz Cruz, Nicolas Norena, Ajeet Kaushik, and Shekhar Bhansali. A low-cost miniaturized potentiostat for point-of-care diagnosis. *Biosensors and Bioelectronics*, 62:249–254, 2014.

[17] João Paulo de Campos da Costa, Wagner Benicio Bastos, Paulo Inacio Da Costa, Maria Aparecida Zaghete, Elson Longo, and João Paulo Carmo. Portable laboratory platform with electrochemical biosensors for immunodiagnostic of hepatitis c virus. *IEEE Sensors Journal*, 19(22):10701–10709, 2019.

[18] Farzan Dehbashi, Ali Abedi, Tim Brecht, and Omid Abari. Verification: can wifi backscatter replace rfid? In *MobiCom'21*, pages 97–107, 2021.

[19] Daniel I Feig, Duk-Hee Kang, and Richard J Johnson. Uric acid and cardiovascular risk. *New England journal of medicine*, 359(17):1811–1821, 2008.

[20] Ana CM Gagliardi, Marcio H Miname, and Raul D Santos. Uric acid: A marker of increased cardiovascular risk. *Atherosclerosis*, 202(1):11–17, 2009.

[21] Wei Gao, Sam Emaminejad, Hnin Yin Yin Nyein, Samyuktha Challa, Kevin Chen, Austin Peck, Hossain M Fahad, Hiroki Ota, Hiroshi Shiraki, Daisuke Kiriya, et al. Fully integrated wearable sensor arrays for multiplexed in situ perspiration analysis. *Nature*, 529(7587):509–514, 2016.

[22] Marco Giannetto, Valentina Bianchi, Silvia Gentili, Simone Fortunati, Ilaria De Munari, and Maria Careri. An integrated iot-wi-fi board for remote data acquisition and sharing from innovative immunosensors. case of study: Diagnosis of celiac disease. *Sensors and Actuators B: Chemical*, 273:1395–1403, 2018.

[23] Zheng Gong, Lubing Han, Zhenlin An, Lei Yang, Siqi Ding, and Yu Xiang. Empowering smart buildings with self-sensing concrete for structural health monitoring. In *SIGCOMM'22*, pages 560–575, 2022.

[24] Xiuzhen Guo, Yuan He, Zihao Yu, Jiacheng Zhang, Yunhao Liu, and Longfei Shangguan. Rf-transformer: a unified backscatter radio hardware abstraction. In *MobiCom'22*, pages 446–458, 2022.

[25] Agrim Gupta, Cédric Girerd, Manideep Dunna, Qiming Zhang, Raghav Subbaraman, Tania Morimoto, and Dinesh Bharadia. Wiforce: Wireless sensing and localization of contact forces on a space continuum. In *18th USENIX Symposium on Networked Systems Design and Implementation (NSDI 21)*, pages 827–844, 2021.

[26] Wenya He, Chunya Wang, Huimin Wang, Muqiang Jian, Wangdong Lu, Xiaoping Liang, Xin Zhang, Fengchun Yang, and Yingying Zhang. Integrated textile sensor patch for real-time and multiplex sweat analysis. *Science advances*, 5(11):eaax0649, 2019.

[27] Chien-Tsai Huang, Mei-Lien Chen, Li-Ling Huang, and I-Fang Mao. Uric acid and urea in human sweat. *Chinese Journal of Physiology*, 45(3):109–116, 2002.

[28] HUAWEI. Huawei wearables, 2022. https://consumer.huawei.com/cn/wearables/.

[29] Md. Nazmul Islam and Robert B. Channon. Chapter 1.3 - electrochemical sensors. In *Bioengineering Innovative Solutions for Cancer*, pages 47–71. Academic Press, 2020.

[30] Kay-Tee Khaw, Sheila Bingham, Ailsa Welch, Robert Luben, Nicholas Wareham, Suzy Oakes, and Nicholas Day. Relation between plasma ascorbic acid and mortality in men and women in epic-norfolk prospective study: a prospective population study. *The lancet*, 357(9257):657–663, 2001.

[31] Choong Sun Kim, Hyeong Man Yang, Jinseok Lee, Gyu Soup Lee, Hyeongdo Choi, Yong Jun Kim, Se Hwan Lim, Seong Hwan Cho, and Byung Jin Cho. Self-powered wearable electrocardiography using a wearable thermoelectric power generator. *ACS Energy Letters*, 3(3):501–507, 2018.

[32] Weon-Guk Kim, Do-Wan Kim, Il-Woong Tcho, Jin-Ki Kim, Moon-Seok Kim, and Yang-Kyu Choi. Triboelectric nanogenerator: Structure, mechanism, and applications. *Acs Nano*, 15(1):258–287, 2021.

[33] Satoru Kodama, Kazumi Saito, Yoko Yachi, Mihoko Asumi, Ayumi Sugawara, Kumiko Totsuka, Aki Saito, and Hirohito Sone. Association between serum uric acid and development of type 2 diabetes. *Diabetes care*, 32(9):1737–1742, 2009.

[34] Ahyeon Koh, Daeshik Kang, Yeguang Xue, Seungmin Lee, Rafal M Pielak, Jeonghyun Kim, Taehwan Hwang, Seunghwan Min, Anthony Banks, Philippe Bastien, et al. A soft, wearable microfluidic device for the capture, storage, and colorimetric sensing of sweat. *Science translational medicine*, 8(366):366ra165–366ra165, 2016.

[35] Shuenn-Yuh Lee, Hao-Yun Lee, Ding-Siang Ciou, Zhan-Xian Liao, Peng-Wei Huang, Yi-Ting Hsieh, Yi-Chieh Wei, Chia-Yu Lin, Meng-Dar Shieh, and Ju-Yi Chen. A portable wireless urine detection system with power-efficient electrochemical readout asic and abts-cnt biosensor for uacr detection. *IEEE transactions on biomedical circuits and systems*, 15(3):537–548, 2021.

[36] Sam Lemey, Sam Agneessens, Patrick Van Torre, Kristof Baes, Jan Vanfleteren, and Hendrik Rogier. Wearable flexible lightweight modular rfid tag with integrated energy harvester. *IEEE Transactions on Microwave Theory and Techniques*, 64(7):2304–2314, 2016.

[37] Hyo-Ryoung Lim, Yun-Soung Kim, Shinjae Kwon, Musa Mahmood, Young-Tae Kwon, Yongkuk Lee, Soon Min Lee, and Woon-Hong Yeo. Wireless, flexible, ion-selective electrode system for selective and repeatable detection of sodium. *Sensors*, 20(11):3297, 2020.

[38] Rongzhou Lin, Han-Joon Kim, Sippanat Achavananthadith, Selman A Kurt, Shawn CC Tan, Haicheng Yao, Benjamin CK Tee, Jason KW Lee, and John S Ho. Wireless battery-free body sensor networks using near-field-enabled clothing. *Nature Communications*, 11(1):1–10, 2020.

[39] Tong-Hong Lin, Jo Bito, Jimmy GD Hester, John Kimionis, Ryan A Bahr, and Manos M Tentzeris. On-body long-range wireless backscattering sensing system using inkjet-/3-d-printed flexible ambient rf energy harvesters capable of simultaneous dc and harmonics generation. *IEEE Transactions on Microwave Theory and Techniques*, 65(12):5389–5400, 2017.

[40] Yan-Ling Liu, Rong Liu, Yu Qin, Quan-Fa Qiu, Zhen Chen, Shi-Bo Cheng, and Wei-Hua Huang. Flexible electrochemical urea sensor based on surface molecularly imprinted nanotubes for detection of human sweat. *Analytical chemistry*, 90(21):13081–13087, 2018.

[41] Veena Misra, Alper Bozkurt, Benton Calhoun, Thomas Jackson, Jesse S Jur, John Lach, Bongmook Lee, John Muth, Ömer Oralkan, Mehmet Öztürk, et al. Flexible technologies for self-powered wearable health and environmental sensing. *Proceedings of the IEEE*, 103(4):665–681, 2015.

[42] Saman Naderiparizi, Mehrdad Hessar, Vamsi Talla, Shyamnath Gollakota, and Joshua R Smith. Towards battery-free hd video streaming. In *NSDI'18*, pages 233–247, 2018.

[43] Simiao Niu, Naoji Matsuhisa, Levent Beker, Jinxing Li, Sihong Wang, Jiechen Wang, Yuanwen Jiang, Xuzhou Yan, Youngjun Yun, William Burnett, et al. A wireless body area sensor network based on stretchable passive tags. *Nature Electronics*, 2(8):361–368, 2019.

[44] Yao Peng, Longfei Shangguan, Yue Hu, Yujie Qian, Xianshang Lin, Xiaojiang Chen, Dingyi Fang, and Kyle Jamieson. Plora: A passive long-range data network from ambient lora transmissions. In *Sigcomm'18*, pages 147–160, 2018.

[45] Vaishnavi Ranganathan, Sidhant Gupta, Jonathan Lester, Joshua R Smith, and Desney Tan. Rf bandaid: A fully-analog and passive wireless interface for wearable sensors. *(IMWUT)*, 2(2):1–21, 2018.

[46] Alexander Scott, Richa Pandey, Survanshu Saxena, Enas Osman, Yingfu Li, and Leyla Soleymani. A smartphone operated electrochemical reader and actuator that streamlines the operation of electrochemical biosensors. *ECS Sensors Plus*, 1(1):014601, 2022.

[47] Joshua R Smith, Alanson P Sample, Pauline S Powledge, Sumit Roy, and Alexander Mamishev. A wirelessly-powered platform for sensing and computation. In *International Conference on Ubiquitous Computing*, pages 495–506. Springer, 2006.

[48] Tingting Sun, Lianjun Wang, and Wan Jiang. Pushing thermoelectric generators toward energy harvesting from the human body: Challenges and strategies. *Materials Today*, 2022.
[49] Vamsi Talla, Bryce Kellogg, Shyamnath Gollakota, and Joshua R. Smith. Battery-free cellphone. *IMWUT*, 1(2):1–20, 2017.
[50] D Travis Thomas, Kelly Anne Erdman, and Louise M Burke. Nutrition and athletic performance. *Med. Sci. Sports Exerc*, 48:543–568, 2016.
[51] TI. Lmp91000, 2022. https://www.ti.com/lit/ds/symlink/lmp91000.pdf?ts=1669707591666&ref_url=https%253A%252F%252Fwww.google.com.hk%252F.
[52] TI. Msp430frx, 2022. https://www.ti.com/lit/ug/slau445i/slau445i.pdf?ts=1670637536722.
[53] TI. Ti energytrace technology, 2022. https://www.ti.com/lit/pdf/SLAU157AP.
[54] Hoang Truong, Shuo Zhang, Ufuk Muncuk, Phuc Nguyen, Nam Bui, Anh Nguyen, Qin Lv, Kaushik Chowdhury, Thang Dinh, and Tam Vu. Capband: Battery-free successive capacitance sensing wristband for hand gesture recognition. In *Sensys'18*, pages 54–67, 2018.
[55] Bo Wang, Chuanzhen Zhao, Zhaoqing Wang, Kyung-Ae Yang, Xuanbing Cheng, Wenfei Liu, Wenzhuo Yu, Shuyu Lin, Yichao Zhao, Kevin M Cheung, et al. Wearable aptamer-field-effect transistor sensing system for noninvasive cortisol monitoring. *Science advances*, 8(1):eabk0967, 2022.
[56] Minqiang Wang, Yiran Yang, Jihong Min, Yu Song, Jiaobing Tu, Daniel Mukasa, Cui Ye, Changhao Xu, Nicole Heflin, Jeannine S McCune, et al. A wearable electrochemical biosensor for the monitoring of metabolites and nutrients. *Nature Biomedical Engineering*, 6(11):1225–1235, 2022.
[57] Yiran Yang, Yu Song, Xiangjie Bo, Jihong Min, On Shun Pak, Lailai Zhu, Minqiang Wang, Jiaobing Tu, Adam Kogan, Haixia Zhang, et al. A laser-engraved wearable sensor for sensitive detection of uric acid and tyrosine in sweat. *Nature biotechnology*, 38(2):217–224, 2020.
[58] Zhanghao Yu, Fatima T Alrashdan, Wei Wang, Matthew Parker, Xinyu Chen, Frank Y Chen, Joshua Woods, Zhiyu Chen, Jacob T Robinson, and Kaiyuan Yang. Magnetoelectric backscatter communication for millimeter-sized wireless biomedical implants. In *MobiCom'22*, pages 432–445, 2022.
[59] Lonzhi Yuan, Can Xiong, Si Chen, and Wei Gong. Embracing self-powered wireless wearables for smart healthcare. In *PerCom*, pages 1–7. IEEE, 2021.